CaNiN: Suppression of electronic instability by interchain coupling

S. Massidda
Institut Romand de Recherche Numérique en Physique des Matériaux, PHB Ecublens, CH-1015 Lausanne, Switzerland

W. E. Pickett
Institut Romand de Recherche Numérique en Physique des Matériaux, PHB Ecublens, CH-1015 Lausanne, Switzerland and Complex Systems Theory Branch, Code 4692, Naval Research Laboratory, Washington, D.C. 20375-5000

M. Posternak
Institut Romand de Recherche Numérique en Physique des Matériaux, PHB Ecublens, CH-1015 Lausanne, Switzerland
(Received 24 January 1991)

CaNiN is a recently discovered compound that interestingly combines one-dimensional (1D) Ni-N chains in an unusual three-dimensional (3D) arrangement. Although the linear chains could be a possible candidate for Peierls instability and, despite the formal d^9 configuration of Ni, this compound is found to remain metallic and paramagnetic down to very low temperatures. We present the results of electronic-structure calculations for CaNiN as obtained with the full-potential linearized-augmented-plane-wave method within the local-density approximation. Our results show that the interchain coupling strongly reduces the tendency towards electronic instabilities by introducing clear 2D and 3D features into the electronic structure of this compound. The states at the Fermi level are dominated by $dp\pi$ antibonding states. The $dp\sigma$ antibonding bands, expected to be the highest band of the d-p complex, are depressed in energy by the interaction with conduction states (including states with interstitial character), and cannot be clearly singled out throughout the Brillouin zone.

I. INTRODUCTION

The discovery of a wide variety of cuprate compounds with high-temperature superconductivity, structural, magnetic, and metal-insulator transitions has led to increased interest in related materials which may also show similar unusual properties. One example of such related compounds is Sr_2VO_4,[1,2] which may be regarded as a charge conjugate analog of the the cuprates (nearly empty d shell rather than a nearly full d shell); another example is the group of ternary nitride compounds that have been synthesized recently.[3,4]

The compound CaNiN recently produced by Chern and DiSalvo[3] is an example of a material which might be expected to possess unusual properties. Its crystal structure, which contains layers of one-dimensional (1D) chains stacked in a three-dimensional (3D) manner, contains strong 1D, 2D, and 3D aspects. Moreover, Ni is formally in the 1+ charge state, i.e., the same formal d^9 configuration characteristic of several of the antiferromagnetic (AFM) insulating copper oxide compounds. The crystal structure (described below) contains 1D aspects arising from the Ni-N chains which are metallic and might be expected to lead via a Peierls instability toward superstructure formation, while the d^9 configuration might be expected to promote magnetic behavior, possibly AFM spin arrangement along the chains. However, Chern and DiSalvo have found the resistivity to be metallic and without anomaly from T=320 K down to 4 K, with a resistivity ratio around 8. The susceptibility is paramagnetic, increasing as the temperature is lowered from 320 K and leveling off below 7 K.

To investigate these questions we have carried out self-consistent local-density calculations of the electronic structure of this compound. Because CaNiN has only recently been synthesized, little is known about its electronic structure. Two other compounds with the same structure are known, YCoC and SrLiN (see Chern and DiSalvo[3]), and the only study has been a Hückel calculation of a $(CoC)^{3-}$ chain reported by Hoffmann, Li, and Wheeler.[5] Their results contained one surprise. For a chain of equally spaced CoC atoms, whose Co d states and C p states lie at roughly the same energy, it is expected that the $dp\sigma$ bonding band should lie lowest and that the $dp\sigma^*$ (antibonding) band should lie highest. This hypothesis was not verified; instead, these authors found that the (degenerate) $dp\pi^*$ antibonding bands were higher than the $dp\sigma^*$ band. This latter band was rather flat, having been repelled strongly by the Co $4s$ state which lies above the d-p complex. The Fermi level crossed only the two $dp\pi^*$ bands, and since the $(CoC)^{3-}$ chain they considered lacks two electrons of filling the d-p complex, the result was two degenerate half-filled $dp\pi^*$ bands. Hoffmann, Li, and Wheeler[5] suggested that the resulting

chain is likely to be magnetic.

The Ni-N chains occurring in CaNiN are similar in many ways to this picture of the CoC chains. Taking Ca as doubly ionized, the analagous situation here is the $(NiN)^{2-}$ chain, which is one electron short of filling the *d-p* band complex. Although much of the basic electronic structure of the chain is similar to that proposed for CoC by Hoffmann, Li, and Wheeler, we find more complex behavior, in at least two respects. First, the $dp\sigma^*$ band indeed interacts strongly with conduction states above, but this interaction takes place primarily with Ca *d* states and with states with a strong interstitial component rather than simply with metal (Ni) *s* states. Second, 2D coupling within a layer splits the two $dp\pi^*$ bands, and 3D coupling mixes the states of the two sets of perpendicular chains, resulting in a more complex Fermi surface with much less inclination toward Fermi surface driven charge-density-wave (CDW) or spin-density-wave (SDW) instabilities. Simply put, interchain coupling strongly reduces the impetus toward electronic instabilities that might have occurred if interchain coupling were smaller.

The paper is organized as follows. In Sec. II the structure of CaNiN is described, and Sec. III presents the calculational methods and details. In Sec. IV we present the band structure, giving particular emphasis on analysis of the states near the Fermi energy E_F in terms of chain-derived bands and interchain coupling. To clarify the nature of the interchain interactions, we present calculations also for a single layer of Ni-N chains. In Sec. V we discuss the Fermi surface (FS) itself and present FS quantities which determine transport properties in metals. A brief review of the results and relationship to other materials is provided in Sec. VI.

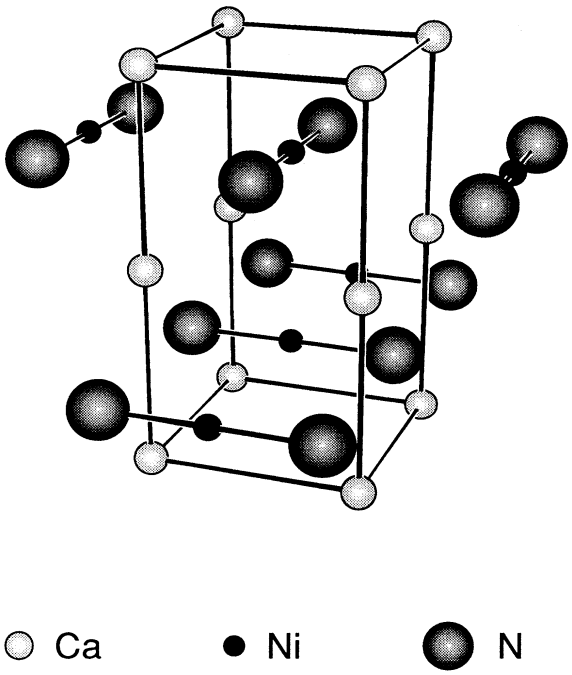

FIG. 1. Perspective view of the crystal structure of $P4_2/mmc$ CaNiN, showing the layers of Ni-N chains separated by square arrays of Ca ions. Note that the Ca ions are tetrahedrally coordinated with four N atoms, two in each of the two neighboring layers. Sphere sizes are proportional to the ionic radii of the elements.

II. CRYSTAL STRUCTURE

CaNiN forms in an unusual crystal structure (see Fig. 1) with tetragonal $P4_2/mmc(D^9_{4h})$ space group (No. 131 in the International Tables). All atoms lie on special sites, so the lattice constants a and c are the only structural parameters. Chern and DiSalvo[3] find $a = 3.5809(2)$ Å and $c = 7.0096(3)$ Å, so $c/a = 1.9575$. Ca occupies the $2e$ positions $(0,0,\frac{1}{4})$, $(0,0,\frac{3}{4})$; Ni occupies the $2b$ positions $(\frac{1}{2},\frac{1}{2},0)$, $(\frac{1}{2},\frac{1}{2},\frac{1}{2})$; N occupies the $2c$ positions $(0,\frac{1}{2},0)$, $(\frac{1}{2},0,\frac{1}{2})$. All sites have orthorhombic *mmm* symmetry.

In this structure there is one short interatomic distance, the Ni-N distance of 1.79 Å in the basal plane. The simplest way to describe the structure is as Ni-N chains with lattice constant a, separated from the neighboring chain also by the distance a. These planar arrays of chains are stacked in the z direction, but are alternately oriented along the x or y directions at layer separations $c/2$, with the Ni atoms sitting on top of each other. These layers are separated by square arrays of Ca ions, each of which is tetrahedrally coordinated with four N atoms (two above and two below) at a distance of 2.50 Å, which is the second shortest interatomic distance in the crystal. The Ni-Ca distance is 3.03 Å, while the Ni-Ni separations are 3.50 Å $= c/2$ between layers and 3.58 Å $= a$ between chains in a single layer.

Already in the crystal structure one can discern 3D aspects in addition to the obvious 1D (chains) and 2D (layers of chains) characters. Since $a \simeq c/2$, both the Ni sites and the Ca sites form nearly simple cubic sublattices. More interesting, however, may be that the stacking of the layers of chains imposes the lattice constant along the chain (a) to be as well the lattice constant separating the chains. Conversely, the spacing of chains may alter somewhat the lattice constant of the chain by applying an internal strain, resulting in a Ni-N spacing which differs from what would be preferred for a single chain.

III. METHOD OF CALCULATION

In our calculations we used the all-electron full-potential linearized augmented plane wave[6] method, within the local-density approximation with the Hedin and Lundqvist[7] form for the exchange-correlation potential. In this method the core states are calculated fully relativistically and updated at each iteration, whereas the valence states are treated semirelativistically. Inside muffin-tin spheres the wave functions as well as the charge density and potential are expanded in terms of spherical (lattice) harmonics up to $l_{max} = 8$. The interstitial expansion of the wave functions included plane

waves with wave vector $|\mathbf{k}+\mathbf{G}| < 3.75$ a.u., providing well-converged energy eigenvalues. The muffin-tin spheres used are $R_{Ca} = 2.5$ a.u., $R_{Ni} = 1.85$ a.u., and $R_N = 1.45$ a.u. Twenty inequivalent special $\mathbf{k}$ points and a Gaussian smearing technique were used for the Brillouin-zone (BZ) integration in the self-consistent iterations. In order to obtain the density of states and to check the accuracy of the Brillouin zone sampling used, we performed one iteration with the self-consistent potential, using forty $\mathbf{k}$ points and a linear tetrahedron scheme. The Fermi level was found to change by ≈ 0.05 eV, and the l-decomposed charges inside muffin-tin spheres were stable within 0.005 electrons. These differences, even if they remained after further iteration within this scheme, are not large enough to change any of the results discussed in this paper. A single energy window was used to treat both N $2s$ bands and the main d-p valence band. By setting the N $2s$ energy parameter at the Fermi level for a test run, we checked that the accuracy of the linear approximation was better than 1 mRy in the whole considered energy range.

IV. ELECTRONIC STRUCTURE

A. General features

First we establish our notation. Throughout this paper we take the zero of energy at the calculated Fermi level E_F. In addition, to avoid confusion we use the convention that the z axis is along the crystal c axis. Since it is instructive to describe orbitals with the Ni-N chain direction chosen as the direction of quantization, we will always discuss the chain directed along the x axis, with d states given then as $d_{3x^2-r^2}$ (σ), d_{xy} and d_{xz} (π), and $d_{y^2-z^2}$ and d_{yz} (δ).

From the formal valence viewpoint, the compound $Ca^{2+}Ni^{+}N^{3-}$ with two formula units per cell will have valence bands composed of Ni d states and N p states, a total of 16 bands in all. Above this complex of bands will lie Ca valence states (s,p,d) and Ni and N s,p states. The valence bands will not be full; the total of 30 valence electrons will leave one band empty or two or more bands partially empty.

This general picture is supported by the band structure along high symmetry directions, shown in Fig. 2, and the total and local densities of states shown in Fig. 3. Not shown in the Figs. 2 and 3 are the N $2s$ bands, located at ≈ 14 eV below E_F and roughly 0.7 eV wide. The lowest 16 bands lie in a 7-eV-wide range, from -6.5 to $+0.6$ eV. The fifteenth and sixteenth bands are unoccupied all along the BZ edge X-M-X, while small pockets of the thirteenth and fourteenth bands are unoccupied at the BZ corner M.

The density of states (DOS) of Fig. 3 shows that the 16 lowest bands are primarily Ni d and N p. Conduction bands in the 2–10-eV range have considerable Ca d character as well as small amounts of other character, especially plane-wave-like interlayer states which we discuss below. The valence bands are not pure Ni d, N p character, but contain certain small amounts of Ca d and Ni s,p character. Related to this mixing of characters is

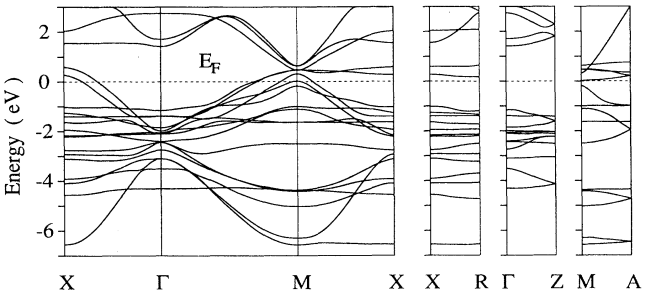

FIG. 2. Energy bands of CaNiN along the high-symmetry directions of the Brillouin zone. The Fermi energy is the zero of energy. $X = (1, 0, 0)\pi/a$, $M = (1, 1, 0)\pi/a$, and the three short panels show dispersion with k_z.

the extension of Ni d character, and especially N p character, into the conduction bands above 1 eV. The N p character in particular extends at least several eV into the conduction bands.

The d-p valence-band complex reflects strong hybridization between the Ni d and N p states. However, these characters are not evenly distributed; the upper

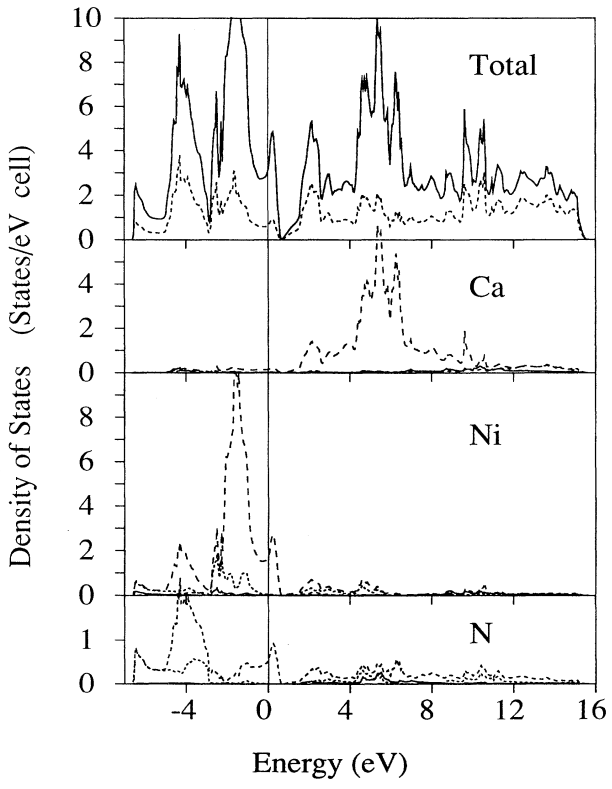

FIG. 3. Total (top panel) and local densities of states of CaNiN. The dashed line in the top panel indicates the interstitial DOS. The various curves are labeled as follows: s, solid curve; p, dashed curve; d, long-dashed curve, $d\sigma$ or $p\sigma$, dotted curve for Ni and N, respectively. Note the change of scale (a factor of 2) for N.

3 eV, which includes the Fermi level, is about 80% Ni d, while the lower 3–4 eV contains more than half N p character. This separation suggests that the N p on-site energy lies lower than the Ni d on-site energy in a tight-binding picture.

Our objective here is to distinguish (i) which features in the electronic structure are due to the Ni-N chain structure itself and therefore are 1D, (ii) which aspects are due to interchain coupling within a layer of chains, (iii) what are the effects of the 2D coupling in the absence of stacking of layers, and finally (iv) what are the effects of interchain coupling between different layers of chains. To facilitate this program, we next describe the electronic structure when the interlayer coupling is removed.

B. Single-layer results

To distinguish clearly between interchain interaction within a layer and between layers, we have performed a calculation in which the layers with Ni-N chains running in the y direction are removed. This doubles the c-axis separation between layers and effectively removes coupling in that direction. To preserve as much symmetry as possible both cations are retained in the original positions (one on each side of the Ni-N layer). To keep the Ni-N band filling approximately the same as in CaNiN, the Ca^{2+} cations were replaced by K^+ cations.

The resulting band structure along the X-Γ-S-Y directions is shown in Fig. 4. In the absence of interchain interaction the bands would be identical along Γ-X and Y-S, and along Γ-S as well if the abscissa were scaled down by $\sqrt{2}$. Breaking of this "symmetry" indicates the strength of interchain interactions within the layer. In addition, for vanishing interchain interaction the $dp\pi$ (d_{xy}-p_y, d_{xz}-p_z) and $d\delta$ ($d_{y^2-z^2}, d_{yz}$) symmetry bands are degenerate. Recall that we choose the x axis as the orbital quantization axis.

The anticipated bands can be considered as one $dp\sigma$ (bonding), one $dp\sigma^*$ (antibonding), two $dp\pi$, two $dp\pi^*$, and two nonbonding $d\delta$ bands, a total of eight bands derived from the five Ni d and three N p states. At X, the lowest band is $dp\sigma$, and the "doublet" near -4 eV is $dp\pi$ with the d_{xz}-p_z partner lying lowest. The interchain interaction affects only the d_{xy}-p_y partner and raises its energy. At Γ, the d and p orbitals are nonbonding by symmetry and the d_{xy}, d_{xz} states are nearly degenerate at ≈ -1.5 eV.

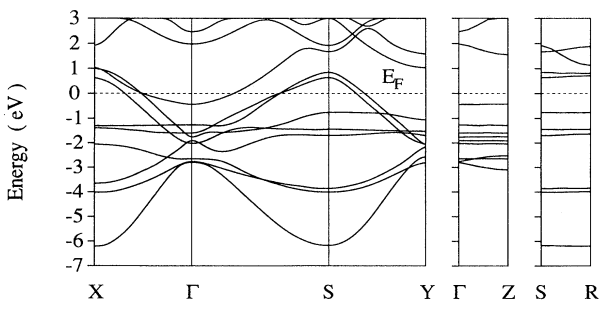

FIG. 4. Energy bands for the "single-layer" K_2NiN calculation. Orthorhombic BZ symmetry labels are used.

We skip the next higher band at X (≈ -2 eV) and return to it below. The next higher "doublet" at X at ≈ -1.3 eV comprises the nonbonding $d\delta$ pair. The two parallel bands which cross E_F along X-Γ are the $dp\pi^*$ bands. These bands are split by $0.3-0.4$ eV across most of the Γ-X line, with the d_{xy}-p_y (in-plane) partner lying higher (similar to the splitting of the bonding $dp\pi$ band discussed above).

It remains to account for the $dp\sigma^*$ character. The band near -2 eV at X (skipped in the discussion above) is primarily of this character, with in addition some other contributions (see below). The band at 1 eV at X and occupied at Γ (-0.4 eV) also has small $dp\sigma^*$ character, as well as K character. This conduction band, which lies above but near the d-p complex throughout the zone and crosses slightly near X, is a mixture of K, Ni s, d, and plane-wave-like (free-electron) interstitial character. The result of the interaction of these conduction states with the $dp\sigma^*$ band is that this band is depressed strongly (to ≈ -2 eV at X) and is relatively dispersionless. The overall energy location of the $dp\sigma$ character is illustrated in Fig. 3 for CaNiN (dotted lines). Also resulting from this hybridization is the mixing in of $dp\sigma^*$ character into the conduction bands above E_F, extending several eV in energy.

The occurrence of a band with large interlayer character so near the d-p band complex is of special interest. It suggests first of all that the work function of a single layer of Ni-N chains, bordered by K atoms, is very low. The character of this band is very reminescent of the interlayer band found in graphite by Posternak *et al.*,[8] which lies at the zone center above the occupied states but below the vacuum zero. These states have only a small atomic component, with most of the density lying between graphite layers. Similar unoccupied states were found by Massidda and Baldereschi[9] in layered intermetallic compound with the AlB_2 structure. States of this kind, slightly above the d-p complex, are also present in CaNiN, as discussed in Sec. IV D.

The depressed, almost dispersionless nature of the $dp\sigma^*$ band is very similar to the behavior found by Hoffmann, Li, and Wheeler,[5] for the $(CoC)^{3-}$ chain. In the case studied by these authors the conduction states consisted of Co s, the only other states in their basis set. Our calculation establishes that essentially the same result holds when a much more extensive basis set is used.

The small dispersion of all valence bands along Γ-Z and S-R in Fig. 4 attests to the small interlayer coupling in this calculation (hence our use of the term "single layer"). A larger k_z dispersion should however be expected for the interlayer bands, based on the experience on graphite and h-BN.[8] However, inspection of the wave functions for the occupied interlayer band (at ≈ -0.4 eV in Fig. 4) and for the next band (at ≈ 2 eV) along Γ-Z shows an interaction of these two bands, resulting in almost dispersionless bands.

We come now to the effects on the Fermi surface and possible electronically driven instabilities. In the absence of interchain interaction (and the interlayer conduction

band crossing E_F which is an artifact of the single-layer system) the $dp\pi^*$ bands along Γ-X are doubly degenerate and half-filled, as found for the $(CoC)^{3-}$ chain by Hoffmann, Li, and Wheeler. Such a situation would strongly indicate a $2k_F$, unit-cell-doubling, CDW or SDW instability. Interchain interactions split these bands, producing two Fermi surface sheets (still reasonably flat) with two competing instabilities, both of which are incommensurate with the lattice. This competition will drastically reduce the tendency toward instability. Thus this single-layer study already provides evidence that 1D features, and accompanying instabilities, are severely weakened by intralayer interchain interactions.

C. Analysis of interlayer chain coupling

Returning to the DOS plots of Fig. 3 for CaNiN, we note that the band edges at -6.5 and 0.6 eV show DOS peaks indicative of broadened 1D square-root singularities arising from bands dispersing along the Ni-N chains. In addition, the DOS peak centered at -1.5 eV is due to the nonbonding $d\delta$ flat bands. Both of these features are remnants of the underlying 1D aspects of the compound, but which are clearly affected by interchain coupling. In the absence of interlayer coupling, the X-Γ panel of Fig. 2 would consist of the bands in the X-Γ panel of Fig. 4 (for the single layer) plus another set of nearly dispersionless bands arising from the perpendicular chains. The $dp\sigma$ (lowest) band and the two $dp\pi^*$ bands (crossing E_F) are very similar in the two panels, but other distinctions are completely obscured by the *interlayer* interactions. While these interactions are not really large, they are of the order of typical band separations in the -5-eV to -1-eV region, i.e., several tenths of an eV, and destroy any simple description of the bands.

Indications of interlayer coupling are provided by the dispersion with k_z (vanishing for no interlayer coupling), which is shown along the X-R, Γ-Z, and M-A lines in Fig. 2. Often the dispersion is small, but within the d-p complex in the -5-eV to -1-eV range, dispersions approaching 1 eV can be seen. The M-A line is particularly instructive, since the nonsymmorphic symmetry operations of the space group lead to strictly doubly degenerate states at A. The connection of bands along M-A allows the identification of pairs of bands which would be degenerate at M for vanishing interlayer coupling, and which (as noted above) are not identifiable from the bands along Γ-M-X-Γ alone.

The isolated state at M at -2.5 eV is mostly composed of Ni $d\delta$ states, showing an interplane Ni-Ni (bonding) interaction. Its partner is the state at -1.1 eV (similar nonbonding character in the a, b directions but antibonding Ni-Ni interplane interaction). The M-A dispersion of these bands is related to this latter interaction, but it is also strongly affected by coupling to unoccupied bands, as discussed later.

This brings us to the complex behavior of the bands near E_F at the zone corner M. It is important to identify the character of these bands which contribute to the Fermi surface, and in addition there is the peculiar behavior of the band at 0.3 eV at M, which shows *very strong* dispersion along the M-A (i.e., k_z) line. To illustrate the character of these bands we present contour plots of their density.

D. Analysis of states near E_F

In Fig. 5 the charge density for the $dp\pi^*$ state at 0.25 eV at X is shown in a (100) plane. It is polarized perpendicular to the layer of chains. From this figure it is evident that the N p states extend to larger distances than do the Ni d states. Thus the interchain interaction within a layer will be larger for N-N than for Ni-Ni coupling.

The charge density for the $dp\pi^*$ states at 0.5 and 0.0 eV at M (becoming degenerate at A) are shown in Fig. 6. The difference between these states, both of which are polarized within the layer, is mostly in the interplane chain coupling (the bonding and antibonding partners actually differ by being, respectively, even and odd relative to the z reflection). The lower-lying state has a stronger bondinglike in-plane N-N interaction between chains, but the plot in the (110) plane cutting the Ca atoms shows a large admixture of interstitial character (orthogonalized to the Ca orbitals) for the bonding state which is missing in the antibonding one. Since the in-plane interactions do not produce dispersion along k_z, and since the direct orbital interaction can be assumed to be negligible for these states polarized in the planes, the ≈ 0.5-eV separation between these two states at M (becoming degenerate at A) can be attributed to the interaction via the interstitial component.

The M state at 0.3 eV (between those just described) is entirely different, as shown by the plot of its density in Fig. 7. Most of this state is interstitial, lacking association with any particular atom. The largest atomic component is its Ca d_{xy} character. It is remarkable that

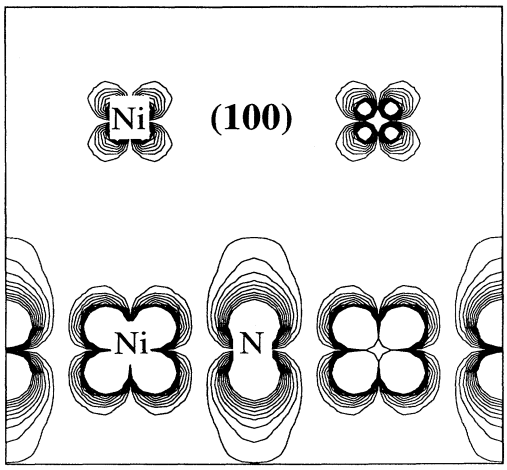

FIG. 5. Contour plot in a (100) plane of the X point state at 0.25 eV above E_F. A Ni-N chain runs horizontally near the bottom of the panel, while the cross section (through Ni) of two chains running perpendicular to the (100) plane is seen at the top of the plot. The antibonding d_{xz}, p_z $dp\pi^*$ character is evident.

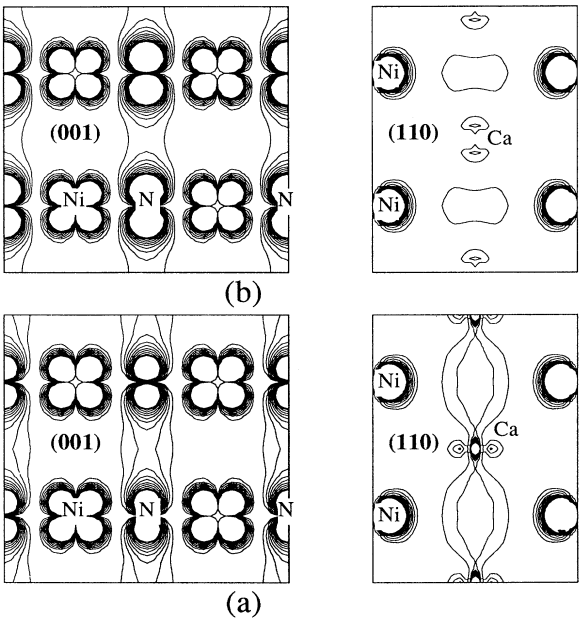

FIG. 6. Contour plots in the (001) and (110) planes of the M states at 0.5 eV (above) and 0.0 eV (below). Two Ni-N chains are shown in the (001) plane. Both are antibonding d_{xy}, p_y $dp\pi^*$ states, but the N-N interchain bonding and the interstitial character is larger for the state at E_F (bottom).

this state avoids the N atoms so effectively that it shows a near z-reflection symmetry relative to the Ca ions in the (100) plane in spite of no such symmetry in the crystal structure (it is violated by the N sublattice).

That such a state of mostly interstitial character can lie so low in energy in this compound is partly attributable to the substantial interstitial volume in this crystal structure. This state interacts strongly with the $dp\sigma^*$ band, nearby in energy, which as a result lies below E_F (at -0.2 eV at M). The interaction of these states is also reflected in their strong, oppositely directed, dispersion with k_z. The question may be raised why this interstitial band is lowest at M, since free-electron-like bands are lowest at Γ. We suggest it is due partially to the Ca d character (d bands generally have their extrema at zone edges) and partially due to the crystal symmetry which may favor a low-energy state at M.

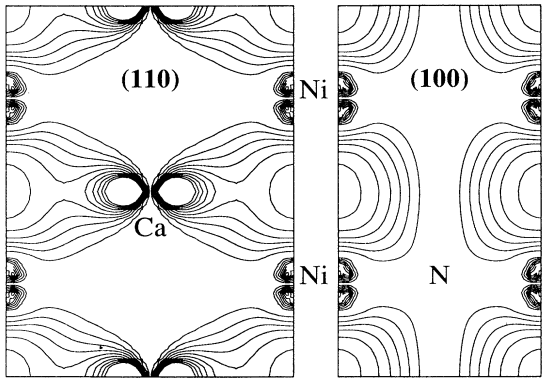

FIG. 7. Contour plots in the (110) and (100) planes of the M band at 0.3 eV which disperses strongly with k_z. This state is primarily interstitial in character but with considerable Ca d_{xy} component.

V. FERMI-SURFACE PROPERTIES

The Fermi-surface cross sections in the Γ-X-M and Z-R-A planes ($k_z = 0$ and $k_z = \pi/c$, respectively) are shown in Fig. 8. They can be seen to arise from two roughly parallel sheets perpendicular to each of the two independent Γ-X directions (one pair arising from each of the layers of chains in the unit cell), but with strong hybridization in the region of crossing. The hybridization and resulting anticrossing is the result of interlayer coupling. The resulting surfaces are four: two large columns of roughly square cross section centered at Γ (Z), and enclosing electrons, and two small columns of roughly

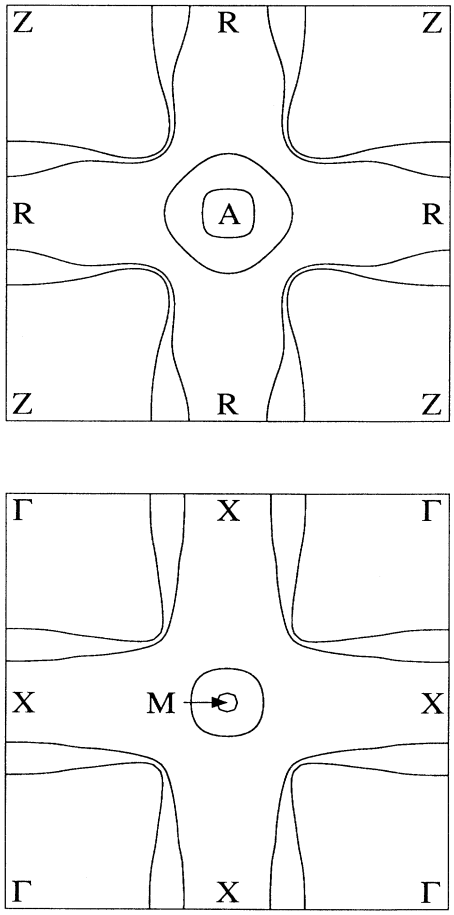

FIG. 8. Fermi surface cross sections of CaNiN in the $k_z = 0$ (lower panel) and $k_z = \pi/c$ (upper panel) planes.

circular cross section centered at M (A) and enclosing holes. The two large electron surfaces can be expected to lead to modest nesting features at $\mathbf{Q} = (0.6\pi/a, 0, 0)$.

The Fermi level DOS $N(E_F)$ is 2.90 states/eV cell for both spins. The rms Fermi velocities are $v_x = v_y = 2.87 \times 10^7$ cm/sec, $v_z = 0.41 \times 10^7$ cm/sec. These quantities determine the Drude plasma energy, defined as

$$\Omega^2_{p,xx} = 4\pi e^2 N(E_F) v_x^2$$

and similarly for y and z components. These quantities are measurable via infrared absorption studies on single crystals. The resulting values are $\hbar\Omega_{p,xx} = \hbar\Omega_{p,yy}$=4.57 eV, $\hbar\Omega_{p,zz}$=0.66 eV. The z conductivity is dominated by the larger circular sheet centered at M which has the larger k_z dispersion.

We have also determined the Hall tensor coefficients $R^H_{\alpha\beta\gamma}$ along the lines reported earlier for copper oxide compounds.[10,11] We find $R^H_{xyz} = 0.39 \times 10^{-11}$ m^3/C, $R^H_{yzx} = R^H_{zxy} = 0.30 \times 10^{-9}$ m^3/C, an anisotropy of nearly 2 orders of magnitude. These larger components correspond to a magnetic field lying in the plane. For all these Hall tensor components there is a cancellation between the holelike contribution of the circular Fermi surfaces (FS) centered around M (A) with the electronlike contribution of the remaining FS. The positive contributions prevail, probably because of the overall low curvature of the electronlike FS, but the resulting R^H_{xyz} is much smaller than the single-band contributions. In the case of $R^H_{yzx} = R^H_{zxy}$ the dominant contribution is given by the larger circular FS around M (having the larger c-axis dispersion as stated before.

VI. DISCUSSION AND SUMMARY

The main features of the electronic structure of CaNiN are the following: (i) 1D aspects are the single most dominant feature. The $dp\sigma$ and $dp\pi$ bonding and antibonding chain bands are readily identifiable. (ii) The $dp\sigma^*$ antibonding band, anticipated to be the highest of the d-p bands, is depressed strongly by interaction with conduction-band states, which are primarily composed of interstitial, plane-wave-like character with a Ca d_{xy} component. (iii) Interchain coupling within the layer of chains removes the degeneracy of the $dp\pi^*$ bands, giving rise to two Fermi surface sheets with incommensurate nesting wave vector rather than a single, doubly degenerate sheet at the commensurate wave vector $\pi/2a$. (iv) Interlayer coupling further removes low-dimensional features especially in the Fermi surface, reducing more the strength of any incipient instability due to Fermi surface nesting. This coupling also contributes to the stability of the crystal structure.

These facts already account qualitatively for the lack of any electronic instability, consistent with the observed metallic behavior from room temperature down to 4 K.[4] The primary channel for interchain coupling seems to be through N-N interactions, either directly in the case of interactions within a layer, or through the Ca ion in the case of interlayer coupling. However, direct Ni-Ni interaction and coupling of both Ni and N states via interstitial states also appear to be important.

Although a Peierls-like CDW or SDW instability is not expected from the calculated band structure, the clear 1D feature of the crystal structure (the Ni-N chains) suggests a possible tendency toward buckling of the chains. Simple buckling rearrangements would not open any gap in the band structure, and therefore would be favored more by entropy considerations than by energetics. Our cursory look into possible structural rearrangements did not result in any obvious symmetry-lowering distortions in this crystal structure.

A remaining question is the approximate d^9 configuration of the Ni ion and possible magnetic order resulting from strong local exchange interaction rather than Fermi surface nesting. The leveling off of the susceptibility below 10 K could be an indication of antiferromagnetic order. We have not investigated such possibilities directly. However, a calculation of the Stoner enhancement factor gives $S = [1 - I N(E_F)]^{-1} = 1.5$, which is not close to a ferromagnetic instability. The Ni sublattice would readily support an AFM state, but the absence of flat bands near E_F and a strong nesting feature suggests a SDW state is not likely.

Note added in Proof. A Gudat *et al.*, J. Less-Common Metals **159**, L29 (1991) have reported an isoelectronic compound BaNiN that contains zig-zag Ni-N chains. The structure does not appear to be intimately related to the CaNiN structure studied here. We thank F. J. DiSalvo for bringing this reference to our attention.

ACKNOWLEDGMENTS

W.E.P. is grateful to F. J. DiSalvo for bringing the CaNiN compound to his attention, and for informative discussions on nitrides. Work was supported by the Swiss National Foundation under Grant No. 20-5446.87.

[1] M.J. Rey, Ph. Dehaudt, J. C. Joubert, B. Lambert-Andron, M. Cyrot, and F. Cyrot-Lackmann, J. Solid State Chem. **86**, 101 (1990).

[2] W. E. Pickett, D. Singh, D. A. Papaconstantopoulos, H. Krakauer, M. Cyrot, and F. Cyrot-Lackmann, Physica B+C **162-164C**, 1433 (1989); D. Singh, W. E. Pickett, R. E. Cohen, D. A. Papaconstantopoulos, H. Krakauer, Physica B+C **163B**, 470 (1990); M. Cyrot *et al.*, J. Solid State Chem. **85**, 321 (1990).

[3] M. Y. Chern and F. J. DiSalvo, J. Solid State Chem. **88**, 459 (1990).

[4] F. J. DiSalvo, Science **247**, 649 (1990); M. Y. Chern and F. J. DiSalvo, J. Solid State Chem. **88**, 528 (1990).

[5] R. Hoffmann, Jing Li, and R. A. Wheeler, J. Am. Chem. Soc. **109**, 6600 (1987).

[6] O. K. Andersen, Phys. Rev. B **12**, 3060 (1975); D. D. Koelling and G. O. Arbman, J. Phys. F **5**, 2041 (1975); D. R. Hamann, Phys. Rev. Lett. **42**, 662 (1979); E. Wimmer, H. Krakauer, M. Weinert, and A. J. Freeman, Phys. Rev. B **24**, 864 (1981); H. J. F. Jansen and A. J. Freeman,

ibid. **30**, 561 (1984).
[7] L. Hedin and B. I. Lundqvist, J. Phys. C **4**, 2064 (1971).
[8] M. Posternak, A. Baldereschi, A.J. Freeman, E. Wimmer, and M. Weinert, Phys. Rev. Lett. **50**, 761 (1983); in *Intercalated Graphite*, edited by M. S. Dresselhaus, G. Dresselhaus, J. E. Fischer, and M. J. Moran, MRS Symposia Proceedings No. 20 (Materials Research Society, Pittsburgh, 1983), p. 117; M. Posternak, A. Baldereschi, A.J. Freeman, and E. Wimmer, Phys. Rev. Lett. **52**, 863 (1984); A. Catellani, M. Posternak, A. Baldereschi, H.J.F. Jansen, and A.J. Freeman, Phys. Rev. B **32**, 6997 (1985).
[9] S. Massidda and A. Baldereschi, Solid State Commun. **66**, 855 (1988); S. Massidda, Ph.D. thesis, Trieste, Italy, 1985.
[10] P. B. Allen, W. E. Pickett, and H. Krakauer, Phys. Rev. B **36**, 3926 (1987); **37**, 7482 (1988).
[11] N. Hamada, S. Massidda, Jaejun Yu, and A.J. Freeman, Phys. Rev. B **42**, 6238 (1990).